AIMS Materials Science, 3(4): 1309-1320.
DOI: 10.3934/matersci.2016.4.1309
Received: 17 August 2016
Accepted: 23 September 2016
Published: 27 September 2016

http://www.aimspress.com/journal/Materials

Research article

Rapid synthesis of thin amorphous carbon films by sugar dehydration and dispersion

Keith E. Whitener Jr. *

Chemistry Division, U. S. Naval Research Laboratory, Washington D. C., 20375, United States

*** Correspondence:** Email: keith.whitener@nrl.navy.mil.

Abstract: We have prepared amorphous carbon films with variable thicknesses down to <5 nm using a simple procedure which takes minutes and employs no special equipment. We prepare a carbonaceous suspension by the dehydration reaction of sulfuric acid with glucose and show that adding this mixture dropwise into water creates a thin carbon film on the water's surface which can be transferred to an arbitrary substrate. This transparent brown film is non-conductive and has a chemical makeup, excluding hydrogen, of $CS_{0.0213}O_{0.4563}$. After brief annealing under 10% H_2 in argon at 800 °C, the film has a high optical contrast and increased conductivity, with a chemical makeup of $CO_{0.0828}$, suggesting that the material has at least short-range graphitic order. We repeat the experiment with chitosan replacing glucose and show using Raman spectroscopy and X-ray photoelectron spectroscopy (XPS) that it is likely that nitrogen incorporates into the graphitic lattice.

Keywords: thin carbon films; acid dehydration; high-temperature annealing; X-ray photoelectron spectroscopy; Raman spectroscopy; atomic force microscopy

1. Introduction

The reaction of ordinary table sugar with sulfuric acid:

$$C_{12}H_{22}O_{11} + H_2SO_{4\,(l)} \rightarrow \text{carbon foam} + H_2SO_{4\,(aq)}$$

is a popular high school chemistry experiment and a dramatic demonstration of the dehydrative power of sulfuric acid [1]. Recently, the scientific community has taken a renewed interest in this classic experiment, using acid dehydration of carbohydrates to create hydrophilic carbonaceous nanodots [2,3,4]. These nanodots have intriguing photoluminescent properties which may find

applications in optoelectronics and photocatalysis [4]. Other groups have used thermal and hydrothermal methods to synthesize carbonaceous species from sugars [5,6]. In addition, significant effort has gone into researching inexpensive syntheses of nanostructured and low-dimensional carbon materials, including graphene [7,8], nanoporous carbons [9,10,11], plasma-produced amorphous carbon thin films [12–15], and carbon molecular sieves [16]. Functionalized nanocarbons show promise in a number of areas including biocompatibility [12,15], chemical catalysis and acid-base reactions [17], as well as the oxygen reduction reaction employed in fuel cells [18].

In this paper, we present a straightforward and rapid method of making thin amorphous carbon films on silica support. We use the simple dehydration reaction of glucose with sulfuric acid presented above to synthesize a carbonaceous suspension which, when pipetted into water, disperses across the surface in a thin continuous film which can be retrieved onto an arbitrary substrate. This brown film is electrically insulating and rich in sulfur and oxygen containing functional groups. Upon rapid annealing at 800 °C, the film loses all of its sulfur content and a large fraction of its oxygen content and its Raman spectrum develops a graphitic peak. The material also displays thickness-dependent conductivity upon annealing. We can also extend this method to other carbohydrates besides glucose. Chitosan, for example, allows the incorporation of nitrogen groups into the carbonaceous material, which are retained even after annealing.

2. Materials and Method

2.1. Preparation of Carbon Suspension

A typical reaction is as follows: 5 mL of concentrated sulfuric acid was added to a 20 mL glass scintillation vial containing 1 g of glucose. The mixture was stirred briefly, then placed on a 200 °C hotplate and swirled vigorously. During this period the colorless mixture first turned yellow, then a deep red-brown, and finally brown and black, coating the walls of the flask with an opaque film, a transformation that took roughly 1 minute. The mixture was then removed from the heat and vigorous swirling was continued until bubbling of the solution subsided. The product was an opaque black viscous liquid (Figure 1a).

2.2. Preparation and Transfer of Carbon Film

A Petri dish was filled with distilled water and a few drops of the carbon suspension were pipetted onto the surface of the water. The bulk of the drops sank to the bottom of the beaker, but a translucent brown film spread out on the water's surface (Figure 1b). This thin film was most easily observed optically at an oblique angle to a light source, where its iridescence could easily be observed. The floating carbon film was transferred onto a piranha-washed Si wafer with a 250 nm thermal oxide layer by scooping the wafer up through the surface of the water (Figure 1c). For optical transmittance, the film was transferred onto a piranha-washed quartz wafer. The wafer was then either allowed to dry in air or spun on a spincoater at 5000 rpm with a 1000 rpm/s acceleration rate for 1 minute to remove excess water from between the wafer and the carbon film. It is important to note that the success of this part of the experiment seems to depend on how far the dehydration has been allowed to progress. If the carbon suspension is dark red or brown, then in general, the sugar has not been sufficiently dehydrated for film formation, and the suspension will be too soluble to

phase-separate into a surface film. If, however, the carbon suspension is black and very viscous, the reaction might have already proceeded too far toward the carbon foam stage, and upon attempting to create the film, the drops will simply sink to the bottom of the petri dish without dispersing at all. Despite these caveats, the formation of the film is a fairly robust process, and the preparation of the carbon suspension is rapid and facile enough to be attempted multiple times without becoming overly tedious.

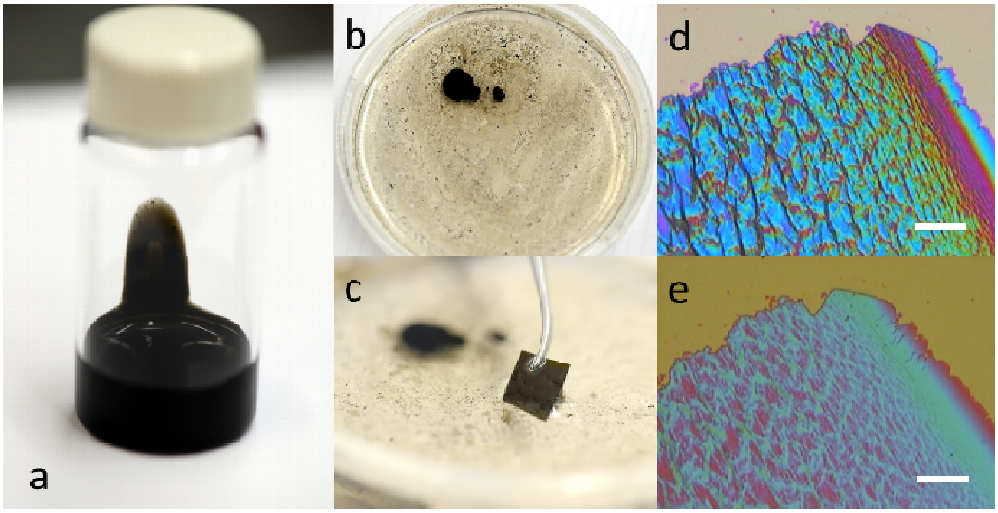

Figure 1. (a) Suspension of dehydrated sugar in concentrated sulfuric acid. Note the opacity of the suspension on the back wall of the scintillation vial. (b) Dispersion of a drop of suspension on water in a Petri dish. The large black blob is the bulk of the drop, and the thin brownish carbon film can be seen on the surface of the water. (c) Deposition of the thin carbon film onto a Si/SiO_x wafer. (d–e) Optical microscopy of unannealed (d) and thermally annealed (e) thin films on Si/SiO_x wafer. The white scale bar is 100 μm.

2.3. Annealing

The sample was annealed in a tube furnace under a continuous 10 sccm gas flow of 10% H_2 in argon. The furnace was ramped up to 800 °C over 10 minutes and held at this temperature for 15 minutes. The heat was then turned off and the sample was cooled without removing the H_2/Ar flow by opening the lid to the oven. After roughly 30 minutes, the sample had cooled to below 100 °C, and it was removed from the tube.

2.4. Characterization

Raman spectra were obtained on a Renishaw spectrometer fitted with a microscope at an excitation wavelength of 514.5 nm provided by an Ar-ion laser. Film thickness measurements were performed using an Asylum atomic force microscope (AFM) in contact mode. Four-probe conductivity measurements were taken on a Keithley 4200-SCS instrument. XPS data was obtained on a Thermo Kalpha spectrometer using the Al Kα line as the X-ray source. For XPS measurements,

a gold-sputtered film on silicon was used as the substrate to allow accurate measurements of oxygen content of the carbon films.

3. Results and Discussion

We carried out the acid dehydration of a carbohydrate (glucose) with an excess volume of sulfuric acid and carefully controlled heating, which prevented a runaway reaction of the sugar and formation of the carbon foam. The resultant liquid consisted of a suspension of carbonaceous particles in sulfuric acid. It was found that a drop of this suspension would disperse in water in such a way that a translucent brown film covered the surface of the water. This film was continuous over millimeters to centimeters, structurally sturdy enough to be transferred onto a silicon wafer. Some of the samples were annealed in a tube furnace at 800 °C under H_2 in argon for 15 minutes plus heating and cooling time. The total time to prepare fully annealed samples was on the order of 1.5 hours, and the equipment used is simple and inexpensive enough to be replicated in a classroom environment. The properties of the annealed and unannealed samples were compared using AFM, Raman spectroscopy, and XPS as well as by examining their conductivities.

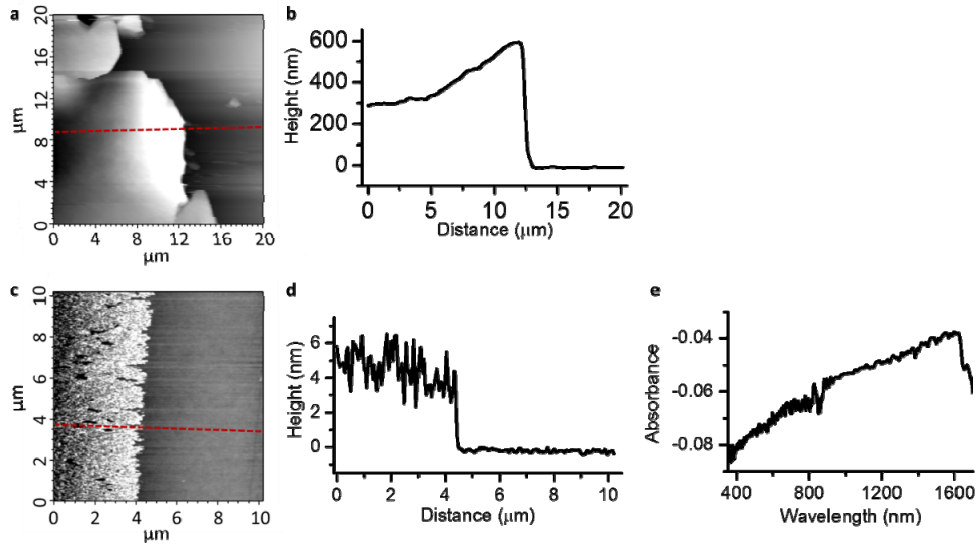

Figure 2. (a) AFM height image of thick annealed amorphous carbon films. (b) Cross section profile of the AFM height image, as indicated by the dashed line from Figure 2a. (c) AFM height image of thin annealed amorphous carbon films. (d) Cross section profile of the AFM height image, as indicated by the dashed red line from Figure 2c, showing the pronounced roughness in the thin films. (e) UV-Visible optical absorbance for 4.69 nm thick film.

Much work has previously been performed on CVD and plasma deposition of amorphous carbon films [14,15,19]. In those cases, film thickness is determined by deposition time. However, in our case, film thickness is related to the duration of the dehydration reaction, with shorter reaction times leading to thinner films. In the description of the results that follow, the thick (~300 nm films) were produced after a 60 second dehydration reaction, whereas the thin (~5 nm films) were produced

after a 30 second dehydration reaction. Both annealed and unannealed films exhibited a range of colors based on their thicknesses (Figures 1d–e). Upon annealing, the thicker films became visibly shinier. The unannealed films were completely non-conductive, whereas after 15 minutes of annealing at 800 °C, the resistance of the films decreased. This resistance was weakly thickness-dependent, with roughly 300 nm variable-thickness films (Figures 2a and 2b) exhibiting an average bulk resistivity of 0.161 ± 0.039 Ω·cm and 4.69 nm films (Figures 2c and 2d) having an average bulk resistivity of 0.572 ± 0.056 Ω·cm. The 4.69 nm thick films showed a pronounced roughness (standard deviation of ±1.78 nm); these films show many similarities to the films generated by Vijapur et al., who performed chemical vapor deposition of brown coal onto copper at high temperatures [19]. We also point out, as shown in Figure 2, that the thinner films have a high roughness but also a high uniformity. In contrast, the thicker films have a lower apparent roughness, but are much less uniform in thickness. This is most dramatically illustrated in Figure 2b, where the thickness of the film varies from 300 to 600 nm over a distance of 10 microns. In addition, 5 nm thick films were transferred onto quartz and thermally annealed to examine optical transmittance. These samples exhibited a broad UV-visible optical absorbance of between 4% and 8%, as shown in Figure 2e, that was quite homogeneous across the film's surface. The absorbance of the thicker film was much less homogeneous because its thickness was significantly less uniform.

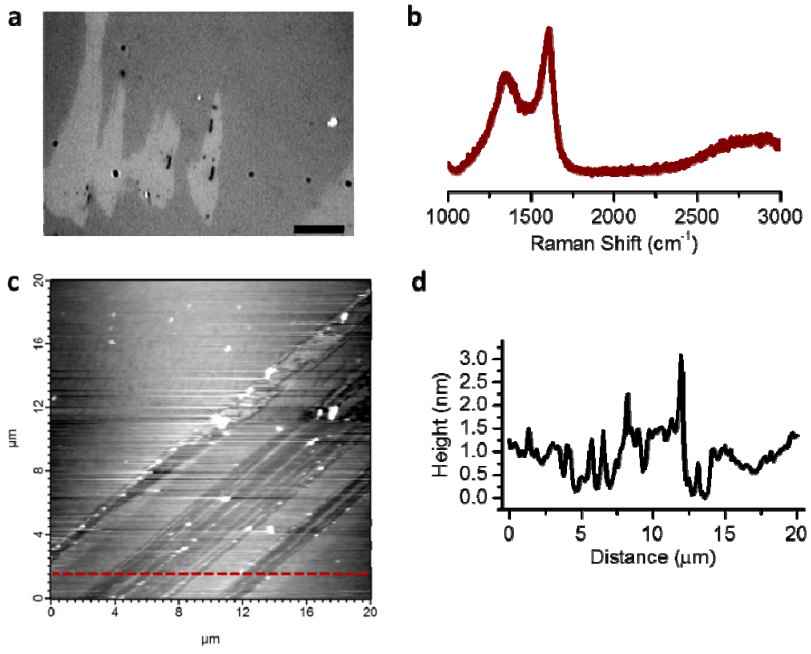

Figure 3. (a) Contrast-enhanced optical image of ultrathin carbon film after anneal. Scale bar is 10 μm. The black spots are likely stray dust particles. (b) Raman spectrum of dark area in optical image, with the signature of amorphous carbon residue. (c) 20 μm × 20 μm AFM topography image of ultrathin carbon films. The films were scratched with tweezers in an attempt to get height measurements. (d) AFM cross section corresponding to the dashed red line in the AFM topography image shown in (c). As the cross section shows, the thickness of the film was comparable to its roughness, thus precluding an accurate measure of film thickness. On average, however, the film was between 1 and 2 nm thick.

In addition, we also observed some very thin films (1–2 nm) which showed enhanced optical contrast as well as Raman signatures for carbon films but whose thickness was roughly the same magnitude as their roughness (0.88 nm), making it difficult to obtain precise thicknesses for them (Figure 3). These ultrathin films were non-conductive even after annealing. The high optical contrast coupled with lack of conductivity indicate that, while these films might have polyaromatic regions large enough to give broadband UV-Vis absorption, the conjugation network is not extensive enough to sustain electrical conductivity. We hypothesize that the films are either not connected at the nanoscale or are connected weakly by non-conjugated sp^3 polymer domains.

The Raman spectrum (Figure 4) of the unannealed film showed a broad background with a weak broad peak at 1595 cm^{-1} and a shoulder at 1475 cm^{-1}. The G peak at 1595 cm^{-1} indicates the presence of sp^2 polyaromatic carbon networks, whereas the origin of the peak at 1475 cm^{-1} is hypothesized to be trans-polyacetylene like chains at grain boundaries. This peak also appears in the Raman spectra of nanodiamonds with significant disorder [20]. In contrast, the Raman spectrum of the annealed film strongly resembled that of graphene oxide, exhibiting broad peaks at 1335 cm^{-1} and 1598 cm^{-1}, corresponding to D and G peaks, respectively. The D/G ratio is the ratio of D peak integrated area to G peak integrated area, and it is an indicator of an interruption of the sp^2 bonding network of graphite on the nanometer scale, either from edges, vacancies, or sp^3 bonded adatoms or point defects [21]. In the case of the films above the D/G ratio was 1.83 ± 0.23, which indicates a significant degree of disorder (less than 1 nm on average between defects). The Raman spectrum strongly resembles that of other disordered pyrolytic carbons [22,23], and differs substantially from multilayer graphene, which shows a much more ordered structure [24].

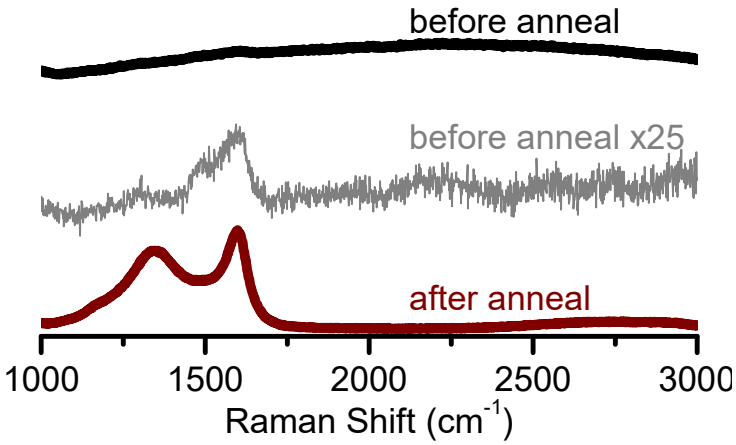

Figure 4. Raman spectra of thin carbon films before and after thermal annealing. The black trace is a film before annealing, and the gray trace is baseline corrected and zoomed in 25x. The red trace is the spectrum of the film after thermal annealing.

XPS spectra of the films (Figure 5) reveal significant differences in chemical composition of the two films. For the unannealed film, a substantial sulfur peak (S2p binding energy = 168.6 eV) was present with an S/C atomic ratio of 0.0213 ± 0.0022, indicating a sulfur atomic content of roughly 1.5%. This sulfur peak was completely absent in the annealed film. In addition, in the unannealed sample, alongside the graphitic carbon peak (284.5 eV), the carbon region of the XPS showed substantial additional contributions from peaks at 286.1 eV and 287.1 eV, indicating the presence of

highly oxidized carbon. These features were largely absent in the annealed sample, where the carbon peak is dominated by its graphitic component. Nevertheless, while the graphitic C1s peak at 284.5 eV was the dominant peak in the annealed film, a significant sp^3 diamondlike carbon peak appeared at 285.8 eV [25,26].

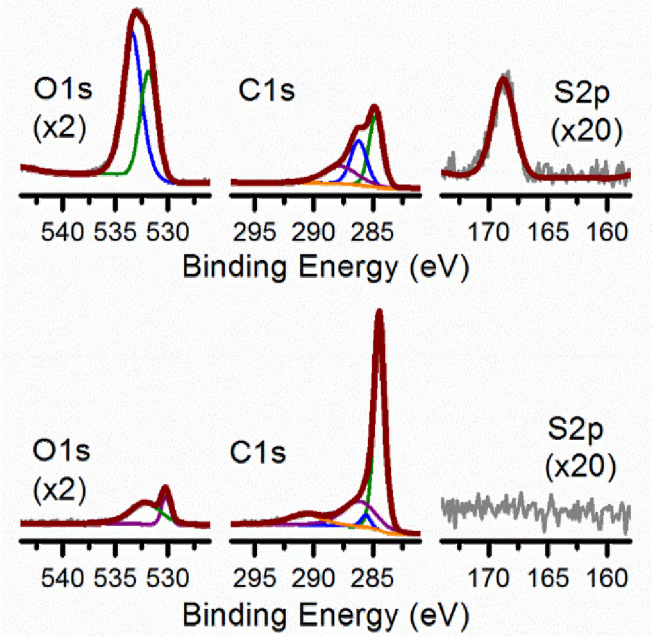

Figure 5. Oxygen, carbon, and sulfur regions of the XPS spectra of unannealed (top row) carbon films and thermally annealed (bottom row) carbon films.

The oxygen region of the XPS provided some interesting features. In order to measure accurately the oxygen content and peak distribution of the samples, the silicon wafers were sputtered with 30 nm of gold and thoroughly cleaned with piranha before the carbon films were transferred to them. The oxygen/carbon ratio of the films decreased from 0.4563 ± 0.0011 in the unannealed samples to 0.0828 ± 0.0318 after annealing, but the peaks in the oxygen region changed significantly upon annealing. The unannealed samples showed two peaks: a broad peak at roughly 532 eV and another at 533.4 eV. After annealing, the peak at 533.4 eV disappeared and a sharp peak at 530.2 eV appeared. Based on the concomitant disappearance of the sulfur peak after annealing, it is likely that much of the oxygen peak at 533.4 eV comes from thermally labile sulfate groups. The peaks at 533.4 eV and 532 eV also represent various oxidized carbon functional groups, including ether, carboxyl, and hydroxyl, as well as adsorbed water. The sharp peak at 530.2 eV most likely corresponds to carbonyl groups, which are less likely to be thermally removed from the carbon film than other oxygen functionalities [25–28].

Carbon thin films containing heteroatoms such as nitrogen have also generated significant interest in the scientific community lately. Several studies suggest that these films could have interesting electrochemical properties, including lowering the kinetic barrier for the oxygen reduction reaction (ORR) in fuel cells [29]. We have attempted to make nitrogen-containing carbonaceous films by replacing glucose in the sulfuric acid dehydrogenation with chitosan, a cheap, abundant, and renewable nitrogen-containing glucosamine polysaccharide generated from crustacean shells. The

preparation of the suspension follows the same procedure, except that a suitable consistency took about 5 minutes to develop instead of 1 minute for glucose. We examined the elemental makeup of both annealed and unannealed samples with XPS, with representative spectra shown in Figure 6. The XPS shows that the sulfur content decreases upon annealing from an S/C ratio of 0.0410 ± 0.0033 to 0.0015 ± 0.0011, similar to what was observed in the case of the glucose-derived films. In addition, the N1s regions of the spectra indicate a significant amount of nitrogen in the film. The unannealed sample has an N/C ratio of 0.1104 ± 0.0023, with a broad prominent peak at 399.5 eV and a shoulder centered at 401 eV. The peak at 399.5 eV is indicative of free amine groups and the peak at 401 eV is generally associated with ammonium cation centers [30]. These observations indicate that the unannealed chitosan-derived carbon film is rich in amine nitrogen groups, a feature that could be useful for attaching organic moieties to the carbon film.

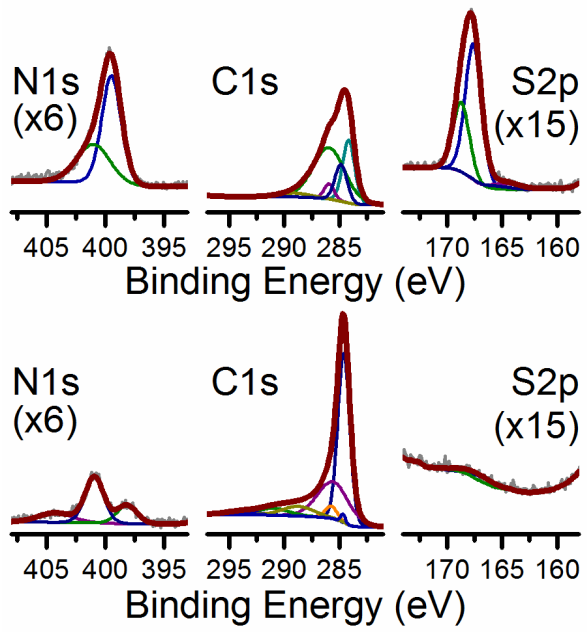

Figure 6. Nitrogen, carbon, and sulfur regions of the XPS spectra of unannealed (top row) and thermally annealed (bottom row) carbonaceous films derived from chitosan.

The XPS spectra of the annealed material further bolster the hypothesis that the peaks observed in the unannealed sample belong to amine and ammonium groups. We would expect amine and ammonium groups to be quite labile at the high temperatures of our annealing process, and indeed, we observe a dramatic reduction in nitrogen content after annealing, with an N/C ratio of 0.0407 ± 0.0011. The XPS peaks are smaller and also have different positions after annealing. The largest peak now appears at 400.5 eV, with a smaller peak at 398 eV and a small shoulder at roughly 404 eV. It is possible that these peaks are residual amine and ammonium peaks, but based on the chemical shift of the peaks, nitrogen might have become incorporated into the sp^2 graphene-like carbon lattice. In fact, pyrrole and pyridine-like nitrogens have been reported at 398 and 400 eV by other groups [31]. The peak at 404 eV provides further evidence for incorporation of nitrogen in the carbon lattice. Nitrogen peaks at 404 eV are rare in XPS databases, but the chemical shift to higher energy would typically indicate oxidized nitrogen. However, it is difficult to imagine a situation

where annealing at 800 °C in a hydrogen gas atmosphere would yield oxidized nitrogen species. Another possibility, which is consistent with the hypothesis that nitrogens are being incorporated into the lattice, is that the peak at 404 eV is a π-π* shake-up satellite, a secondary excitation of electrons in the carbon lattice from the valence band to the conduction band as a result of the energetic ejection of the core electron by the X-rays [32].

In addition, the Raman spectra of the annealed chitosan-derived carbon film showed significant similarities to the glucose-derived films, in that both demonstrate the large and broad D and G peaks that indicate the presence of sp^2 carbons and high defect density in the graphitic carbon planes. However, looking at the Raman spectra of the films in Figure 7, both the D and G peaks of the chitosan films (1355 cm^{-1} and 1602 cm^{-1}, respectively) show a non-negligible shift to higher energies compared with the glucose films (1335 cm^{-1} and 1598 cm^{-1}, respectively). It has been shown that highly hole- or electron-doped graphene exhibits considerable shifts in Raman peak positions, and that nitrogen-doped graphene shows similar Raman shifts [29]. One would also expect oxygen-bearing functional groups to dope the carbon films as well, but these are present both in chitosan-derived and glucose-derived films to a similar extent. Thus, the Raman spectra of the chitosan-derived carbon films show peak shifts consistent with nitrogen doping of the graphitic lattice.

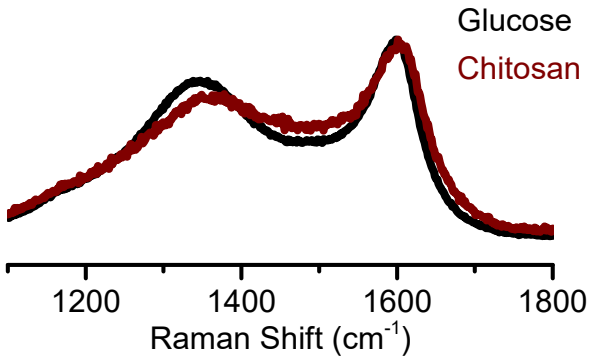

Figure 7. D–G regions of the Raman spectra for glucose-derived (black) and chitosan-derived (red) carbon films. Note the shift of the chitosan-derived spectrum to slightly higher frequencies.

We noted in the introduction that the acid-mediated dehydration of sugar has a long history, both as a classroom demonstration and as an object of intensive scientific study. The reaction mechanism is complex, but we speculate that it begins with elimination and rearrangement reactions through a hydroxymethylfurfural pathway [33]. The sulfuric acid removes H_2O units from the sugar, resulting in extensively sp^2 bonded molecular precursors such as hydroxymethylfurfural. These precursors then most likely dehydratively polymerize and coalesce into larger polyaromatic species. This sequence of events is reflected in our observations, in particular of the Raman spectrum of the unannealed films. For shorter dehydration times, the Raman spectra are essentially featureless with a broad high background. For longer dehydration times, the G peak begins to develop along with a shoulder at 1475 cm^{-1} that is attributed to the development of conjugated polyacetylene chains. Upon annealing, the characteristic disordered graphitic oxide spectrum appears, but the conductivity of the material decreases with thickness and eventually disappears. We hypothesize that the atomic

structure of the films resembles the "house of cards" model that Franklin put forth to describe her X-ray crystallography observations of non-graphitizing carbons derived from pyrolyzed sugar [34]. In this model, small (~5 nm) domains of graphitic carbon are randomly oriented and are weakly linked by non-graphitic carbon chains. Indeed, while graphitizing carbons tend to be quite soft (cf. HOPG), our carbons are hard and brittle, which can be easily seen by scraping the film with a set of forceps. This brittleness is attributable to the strong cross-linking and random orientations of nanocrystalline graphite.

4. Conclusions

We have presented a novel method for preparing thin films of carbon rapidly and without specialized equipment using a simple acid dehydration of glucose. These carbon films can be made conductive by a rapid thermal annealing. In addition, their chemical makeup can be tuned by choosing different starting carbohydrates. For instance, if chitosan, a polyglucosamine, is used in place of glucose, our results suggest that one can obtain carbon films with a significant nitrogen fraction incorporated into the graphitic lattice. These films might find use in chemical catalysis, specifically in catalyzing the oxygen reduction reaction which is necessary for efficient fuel cells.

Acknowledgment

K.E.W. acknowledges a fellowship from the National Research Council for this work.

Conflict of Interest

The author declares no conflicts of interest in this work.

References

1. Tro NJ (2011) *Chemistry: A Molecular Approach*, 2nd ed., Pearson Prentice Hall: Upper Saddle River, NJ, 1013.
2. Zhang J, Shen W, Pan D, et al. (2010) Controlled synthesis of green and blue luminescent carbon nanoparticles with high yields by the carbonization of sucrose. *New J Chem* 34: 591–593.
3. Peng H, Travas-Sejdic J (2009) Simple aqueous solution route to luminescent carbogenic dots from carbohydrates. *Chem Mater* 21: 5563–5565.
4. Li H, Kang Z, Liu Y, et al. (2012) Carbon nanodots: synthesis, properties and applications. *J Mater Chem* 22: 24230–24253.
5. Pan F, Jin J, Fu X, et al. (2013) Advanced oxygen reduction electrocatalyst based on nitrogen-doped graphene derived from edible sugar and urea. *ACS Appl Mater Inter* 5: 11108–11114.
6. Gupta SS, Sreeprasad TS, Maliyekkal SM, et al. (2012) Graphene from sugar and its application in water purification. *ACS Appl Mater Inter* 4: 4156–4163.
7. Ruiz-Hitzky E, Darder M, Fernandes FM, et al. (2011) Supported graphene from natural resources: Easy preparation and applications. *Adv Mater* 23: 5250–5255.
8. Ruan G, Sun Z, Peng Z, et al. (2011) Growth of graphene from food, insects, and waste. *ACS Nano* 5: 7601–7607.

9. Kubo S, White RJ, Yoshizawa N, et al. (2011) Ordered carbohydrate-derived porous carbons. *Chem Mater* 23: 4882–4885.
10. Yu C, Fan J, Tian B, et al. (2002) High-yield synthesis of periodic mesoporous silica rods and their replication to mesoporous carbon rods. *Adv Mater* 14: 1742–1745.
11. Titirici MM, Antonietti M (2010) Chemistry and materials options of sustainable carbon materials made by hydrothermal carbonization. *Chem Soc Rev* 39: 103–116.
12. Javid A, Kumar M, Yoon S, et al. (2016) Role of surface-electrical properties on the cell-viability of carbon thin films grown in nanodomain morphology. *J Phys D Appl Phys* 49: 264001.
13. Javid A, Kumar M, Han JG (2015) Nanoscale surface conductivity analysis of plasma sputtered carbon thin films. *RSC Adv* 5: 96360–96365.
14. Kumar M, Piao JX, Jin SB, et al. (2016) Low temperature plasma processing for cell growth inspired carbon thin films fabrication. *Arch Biochem Biophys* 605: 41–48.
15. Piao JX, Kumar M, Javid A, et al. (2016) Pulsed DC-plasma sputtering induced synthesis of hydrogenated carbon thin films for L-929 cell cultivation. *Surf Coat Tech*.
16. Ryoo R, Joo SH, Jun S (1999) Synthesis of highly ordered carbon molecular sieves via template-mediated structural transformation. *J Phys Chem B* 103: 7743–7746.
17. Su C, Loh KP (2012) Carbocatalysts: Graphene oxide and its derivatives. *Acc Chem Res* 46: 2275–2285.
18. Qu L, Liu Y, Baek JB, et al. (2010) Nitrogen-doped graphene as efficient metal-free electrocatalyst for oxygen reduction in fuel cells. *ACS Nano* 4: 1321–1326.
19. Vijapur SH, Wang D, Botte GG (2013) The growth of transparent amorphous carbon thin films from coal. *Carbon* 54: 22–28.
20. Ferrari AC, Robertson J (2001) Origin of the 1150 cm^{-1} Raman mode in nanocrystalline diamond. *Phys Rev B* 63: 121405.
21. Jorio A, Dresselhaus M, Saito R, et al. (2011) *Raman Spectroscopy in Graphene Related Systems*, Wiley-VCH: Weinheim, Germany.
22. Kaplas T, Kuzhir P (2016) Ultra-thin graphitic film: Synthesis and physical properties. *Nanoscale Res Lett* 11: 1–6.
23. Kaplas T, Svirko Y (2012) Direct deposition of semitransparent conducting pyrolytic carbon films. *J Nanophotonics* 6: 061703–061703.
24. Ferrari AC, Basko DM (2013) Raman spectroscopy as a versatile tool for studying the properties of graphene. *Nat Nanotechnol* 8: 235–246.
25. Zhou JH, Sui ZJ, Zhu J, et al. (2007) Characterization of surface oxygen complexes on carbon nanofibers by TPD, XPS and FT-IR. *Carbon* 45: 785–796.
26. Desimoni E, Casella GI, Morone A, et al. (1990) XPS determination of oxygen-containing functional groups on carbon-fibre surfaces and the cleaning of these surfaces. *Surf Interface Anal* 15: 627–634.
27. López GP, Castner DG, Ratner BD (1991) XPS O1s binding energies for polymers containing hydroxyl, ether, ketone and ester groups. *Surf Interface Anal* 17: 267–272.
28. Plomp AJ, Su DS, Jong KPD, et al. (2009) On the nature of oxygen-containing surface groups on carbon nanofibers and their role for Platinum deposition—An XPS and titration study. *J Phys Chem C* 113: 9865–9869.
29. Wang H, Maiyalagan T, Wang X (2012) Review on recent progress in nitrogen-doped graphene: Synthesis, characterization, and its potential applications. *ACS Catal* 2: 781–794.

30. Shao Y, Zhang S, Engelhard MH, et al. (2010) Nitrogen-doped graphene and its electrochemical applications. *J Mater Chem* 20: 7491–7496.
31. Kondo T, Casolo S, Suzuki T, et al. (2012) Atomic-scale characterization of nitrogen-doped graphite: Effects of dopant nitrogen on the local electronic structure of the surrounding carbon atoms. *Phys Rev B* 86: 035436.
32. Lahaye J, Nanse G, Bagreev A, et al. (1999) Porous structure and surface chemistry of nitrogen containing carbons from polymers. *Carbon* 37: 585–590.
33. Choudhary V, Burnett RI, Vlachos DG, et al. (2012) Dehydration of Glucose to 5-(Hydroxymethyl)furfural and Anhydroglucose: Thermodynamic Insights. *J Phys Chem C* 116: 5116–5120.
34. Franklin RE (1951) Crystallite Growth in Graphitizing and Non-Graphitizing Carbons. *Proc R Soc Lond A Math Phys Sci* 209: 196–218.

AIMS Press